ELSEVIER

Chemical Geology 174 (2001) 333–347

CHEMICAL GEOLOGY
INCLUDING
ISOTOPE GEOSCIENCE

www.elsevier.com/locate/chemgeo

The solubility of H_2O and CO_2 in rhyolitic melts in equilibrium with a mixed CO_2–H_2O fluid phase

Nathalie Tamic *, Harald Behrens, François Holtz

Institut für Mineralogie, Universität Hannover, Welfengarten 1, D-30167 Hannover, Germany

Accepted 9 February 2000

Abstract

H_2O and CO_2 solubilities in a natural rhyolite melt (Erevan Dry Fountain (EDF), Armenia) in equilibrium with H_2O–CO_2 fluids were determined at 200 and 500 MPa and at 800°C and 1100°C. The composition of the fluid phase after experiment was determined by gravimetry, except for extreme CO_2-rich fluids for which mass balance was used. Water and CO_2 contents of the glasses were measured using IR spectroscopy. At 200 MPa, the water solubility changes from a square root dependence on mole fraction of H_2O in the fluid phase ($X^f_{H_2O}$) at low $X^f_{H_2O}$ to a linear dependence above $X^f_{H_2O} = 0.25$. Up to about 5 wt.% dissolved water in the melt (corresponding to $X^f_{H_2O} \approx 0.5$), a similar trend is observed at 500 MPa. At higher $X^f_{H_2O}$, however, the dependence of water solubility on $X^f_{H_2O}$ is more pronounced than at 200 MPa. A negative temperature dependence of water solubility is observed in the whole experimental range at 200 MPa (e.g. the water solubility at $X^f_{H_2O} = 1$ decreases from 5.97 to 5.58 wt.% when temperature rises from 800°C to 1100°C). In contrast, at 500 MPa the temperature dependence of water solubility changes from positive at high $X^f_{H_2O}$ (e.g., increase from 9.84 to 11.04 wt.% for a temperature increase from 800 to 1100°C) to negative at low $X^f_{H_2O}$. An empirical model to predict water solubility in rhyolitic melts in the P–T range 75–500 MPa and 800–1100°C was derived from our new solubility data and data from Blank et al. (1993). The model reproduces the data at 75 and 200 MPa within $\pm 2.5\%$ relative and the data at 500 MPa within $\pm 5\%$ relative.

The CO_2 solubility shows a non-linear dependence on $X^f_{H_2O}$ with deviation from linearity, which increases with pressure. The maximum CO_2 solubilities (equilibrium with pure CO_2) predicted from the data trends are 0.11 ± 0.01 and 0.28 ± 0.03 wt.% at 1100°C and 200 Mpa and 500 MPa, respectively. The temperature dependence of CO_2 solubility is found to be almost negligible at 200 MPa and slightly positive at 500 MPa. Our solubility data at 200 MPa are reproduced slightly better by the model of Papale (1999) than by that of Holloway and Blank (1994).

Keywords: Rhyolitic melt; Water solubility; CO_2 solubility; Infrared spectroscopy; Mixed fluid

1. Introduction

Volatiles (especially water) dissolved in silicate melts influence dramatically the chemical and physical properties of magmas. Because of its high solu-

* Corresponding author. Tel.: +49-511-762-4753; fax: +49-511-762-3045.

E-mail address: n.tamic@mineralogie.uni-hannover.de (N. Tamic).

0009-2541/01/$ - see front matter
PII: S0009-2541(00)00324-7

bility in silicate melts, water is of particular interest for understanding properties of magmas. Water solubility in rhyolitic melts coexisting with pure H_2O fluid was investigated by several authors in the last decades (see McMillan, 1994; Zhang, 1999) using different techniques (see reviews in Ihinger et al., 1994; Kohn, 2000). CO_2 is the second most important volatile which is usually present in natural magmas. The CO_2 solubility in rhyolitic melts is not as well documented as the H_2O solubility (see Blank and Brooker, 1994) because it is significantly lower than that of water. Its presence reduces water solubility significantly (e.g., Blank et al., 1993) and can influence degassing processes. To model degassing during volcanic eruptions, a detailed knowledge of mixing properties of volatile components in the fluid and in the melt is required. So far, only a few studies have been performed to investigate the solubility of volatiles in rhyolitic or in synthetic analogs in equilibrium with mixed fluids melts (e.g., Wyllie and Tuttle, 1959; Kadik et al., 1972; Blank et al., 1993; Schmidt et al., 1998, 1999). Because of the lack of experimental data, the solubilities of H_2O and CO_2 are often calculated using the model of Holloway and Blank (1994). However, the application of this model is limited to relatively low pressure (< 200 MPa). An alternative to this model is that of Papale (1999), which has not been tested experimentally in the pressure range 200–500 MPa.

In this paper, the solubility of H_2O and CO_2 was investigated at 200 and 500 MPa and 800 and 1100°C to constrain the solubility behaviour of mixed fluids in melts of rhyolitic compositions. An empirical model to calculate the H_2O content of the melt between 75 and 500 MPa as a function of the fluid phase composition, pressure and temperature is derived from our new data and solubility data from Blank et al. (1993).

2. Sample preparation

2.1. Starting material

The starting material was an obsidian from Erevan Dry Fountain (EDF), Armenia. The glass was chosen because it contains only minor amount of crystals (less than 1 vol.%), very few bubbles, and little iron. Genesis and rheological properties of the EDF obsidian are described by Bagdassarov and Dingwell (1993) and Stevenson et al. (1995). The composition of the glass is almost metaluminous (Table 1), close to the natural rhyolitic compositions investigated by Blank et al. (1993) and Fogel and Rutherford (1990) and close to well characterised synthetic quartzofeldspathic compositions (such as HPG8 and AOQ, e.g. Hess et al., 1995; Holtz et al., 1995; Dingwell et al., 1998). A water content of the obsidian of 0.22 wt.% was derived from the peak height of the near infrared combination band at 4520 cm^{-1} using the calibration of Zhang et al. (1997). A similar value (0.24 wt.% H_2O) was obtained from the peak height of the fundamental OH vibration band at 3550 cm^{-1} band using a linear molar absorption coefficient of 78 l mol^{-1} cm^{-1} determined for haplogranitic glasses (Behrens and Schmidt, 1998). No CO_2 was detected by IR spectroscopy in the EDF starting glass. Sulfur content was analysed at the CRPG-CNRS (Nancy, France) using coulometric titration and was found to be below the detection limit (50 ppm).

2.2. Experimental procedure

Small glass pieces ($1.5 \times 2.5 \times 5.5$ and $1 \times 2 \times 5$ mm, approximately 45–30 mg) were loaded with a CO_2 source and double-distilled water into a noble metal capsule (Au or Pt, inner diameter, 3–4 mm; wall thickness, 0.2 mm; length, 2–4.5 cm). The proportion of fluid in the charge ranged from 6 to 23

Table 1
Composition of starting material

	EDF	Standard deviation
SiO_2	77.04	0.77
TiO_2	0.11	0.01
Al_2O_3	12.76	0.13
FeO	0.68	0.07
MnO	0.07	0.01
MgO	0.08	0.01
CaO	0.58	0.06
Na_2O	4.07	0.20
K_2O	4.79	0.24
H_2O[a]	0.22	
Total	100.40	

[a]The initial total H_2O content of the natural glass was determined by IR spectroscopy. See text for more details.

Table 2
Experimental conditions and sample characterisation

Sample	CO_2 source[a]	Run duration (h)	P (MPa)	T (°C)	$X^f_{H_2O}$	$X^f_{CO_2}$	C_{water}, KFT (wt.%)
Ech1[b,c]	1	240	200	800	0.288 (19)	0.692 (29)	–
Ech7[b,c]	1	283	200	800	0.355 (18)	0.625 (29)	–
Ech6[c]	1	260	200	800	0.482 (15)	0.498 (26)	–
Ech2[c]	1	240	200	800	0.496 (16)	0.484 (27)	3.84 (07)
Ech8[c]	1	283	200	800	0.571 (17)	0.409 (28)	3.78 (07)
Ech9	1	227	200	800	0.658 (15)	0.322 (26)	4.32 (07)
Ech10[c]	1	227	200	800	0.768 (15)	0.212 (26)	5.01 (07)
Ech3	–	240	200	800	1.000 (10)	0.000 (22)	6.12 (07)
Ech4	–	240	200	800	1.000 (20)	0.000 (–)	6.10 (07)
Ech66	1^+	208	200	1100	0.021 (35)	0.959 (43)	–
Ech65	1^+	208	200	1100	0.102 (32)	0.878 (40)	–
Ech64	1^+	208	200	1100	0.206 (30)	0.774 (39)	–
Ech63	1^+	208	200	1100	0.310 (27)	0.670 (36)	–
Ech62	1^+	208	200	1100	0.410 (24)	0.570 (34)	–
Ech17	2	72	200	1100	0.520 (14)	0.460 (26)	–
Ech18	2	72	200	1100	0.613 (13)	0.367 (24)	3.74 (07)
Ech19	2	72	200	1100	0.706 (11)	0.274 (23)	4.14 (07)
Ech20	2	72	200	1100	0.779 (11)	0.201 (23)	–
Ech21	–	72	200	1100	1.000 (21)	0.000 (–)	–
Ech37	1	98	500	800	0.408 (14)	0.572 (26)	5.02 (07)
Ech38	1	98	500	800	0.433 (14)	0.547 (26)	5.21 (07)
Ech39	1	96	500	800	0.626 (14)	0.354 (25)	6.47 (07)
EDF (1)[d]	–	144	500	800	1.000 (–)	0.000 (–)	9.84 (15)
Ech75	1^+	120	500	1100	0.017 (26)	0.963 (35)	–
Ech74	1^+	120	500	1100	0.084 (24) [0.049]	0.896 (34) [0.931]	–
Ech73	1^+	120	500	1100	0.107 (24) [0.077]	0.873 (34) [0.903]	–
Ech72	1^+	120	500	1100	0.114 (24) [0.085]	0.866 (34) [0.896]	–
Ech59	1^+	156	500	1100	0.120 (30)	0.860 (39)	–
Ech71	1^+	120	500	1100	0.122 (24)	0.858 (34)	–
Ech58	1^+	156	500	1100	0.245 (28)	0.735 (37)	–
Ech57	1^+	156	500	1100	0.374 (25)	0.606 (35)	–
Ech11[e]	1	96	500	1100	0.471 (17)	0.509 (28)	4.83 (11)
Ech22[f]	2	72	500	1100	0.480 (14)	0.500 (26)	–
Ech56	1^+	156	500	1100	0.558 (21)	0.422 (31)	–
Ech61	1^+	156	500	1100	0.672 (16)	0.308 (27)	–
Ech24[f]	2	72	500	1100	0.682 (12)	0.298 (24)	–
Ech41	2	96	500	1100	0.734 (11)	0.246 (23)	7.25 (07)
Ech36	2	96	500	1100	0.837 (09)	0.143 (22)	8.96 (07)
Ech49	–	96	500	1100	1.000 (–)	0.000 (–)	11.04 (06)

C_{water}, KFT is the concentration of total water in the glass determined by KFT. Uncertainty of pressure is ± 5 MPa and uncertainty of temperature is ± 10°C. The $X^f_{H_2O}$ and $X^f_{CO_2}$ given in square brackets correspond to the values obtained by mass balance calculation. See text for more details.

[a] CO_2 was generated in three different ways by decomposition of inorganic materials: (1) silver oxalate was added directly to the sample; (1^+) silver oxalate was placed in a separate unwelded capsule beside the sample; and (2) dehydrated oxalic acid was directly added to the sample.

[b] Glass partially crystallised (< 10 vol.%).

[c] Quenched glass contains aggregates of metallic silver.

[d] Data from Behrens and Jantos (2000).

[e] Dark-coloured glass due to dissolution of silver (up to 2 wt.%).

[f] Sample contains bubbles (< 10 vol.%).

wt.%. Different techniques were used to generate CO_2 during the experiment depending on run temperature. For runs at 800°C, silver oxalate ($Ag_2C_2O_4$) was loaded directly into the Au capsule. In runs at 1100°C, Pt capsules were used and we found that Ag produced by decomposition of silver oxalate formed an alloy with the Pt capsules, which can lead to the leakage of capsules. Therefore, silver oxalate was isolated from the external capsule wall and was loaded into a second small Pt capsule (wall thickness, 0.1 mm, inner diameter, 2.5 mm; length, 10–15 mm), which was carefully squeezed at both ends and placed beside the glass block. An alternative source of CO_2 is oxalic acid ($H_2C_2O_4$), produced by dehydration of $H_2C_2O4 \cdot 2H_2O$ in a drying oven at 105°C. Oxalic acid can be loaded directly in Pt capsules because only volatiles (H_2 and CO_2) are generated by thermal decomposition. CO_2 sources were stored in a desiccator to prevent any water adsorption. However, some remaining water (<1 wt.%) cannot be avoided. During welding, the capsules were cooled using liquid nitrogen to prevent any loss of water or CO_2. For each sample, the technique used to generate CO_2 is specified in Table 2.

2.3. Run conditions

Four sets of experiments were performed, 200 MPa/800°C, 200 MPa/1100°C, 500 MPa/800°C, and 500 MPa/1100°C with run durations ranging from 3 to 12 days (Table 2). Two different kinds of pressure vessels were used: (1) cold seal pressure vessel (CSPV), pressurised with water at 800°C and (2) vertically oriented internally heated pressure vessel (IHPV), pressurised with argon at 1100°C (Becker et al., 1998). Temperature was measured with an accuracy of ± 10°C (taking temperature gradients and accuracy of thermocouples into account) using K-type thermocouples and pressure with an accuracy of ± 5 MPa using a strain gauge manometer.

The oxygen fugacity in CSPV was buffered by the Ni–NiO (NNO) assemblage. An intrinsic oxygen fugacity (expressed as $\Delta \log f_{O_2}$) of NNO + 2.3 was determined at 500 MPa and 850°C in the IHPV by Wilke and Behrens (1999) using Ni–Pd solid sensors (Taylor et al., 1992). The same technique was applied at 500 MPa and 1100°C, and the calculated intrinsic oxygen fugacity was NNO + 3.5.

In CSPV, samples were quenched from experimental conditions to room conditions using a flux of compressed air and the initial cooling rate is approximately 200°C min^{-1}. In IHPV, samples were quenched by turning off the power resulting in an initial cooling rate of 150°C min^{-1}. All runs were quenched isobarically.

3. Analytical techniques

3.1. Determination of the fluid composition after experiment

The fluid composition after the experiment was determined by weighing the capsule using the following procedure: (1) the capsule was weighed; (2) the water from the fluid phase was frozen using liquid nitrogen; (3) the capsule was punctured with a needle; (4) after warming to room temperature, the capsule was weighed to determine the mass of CO_2 ($+N_2$ from air enclosed during loading the capsule); and (5) the capsule was placed into a drying oven and subsequently weighed to determine the mass of water. The capsule weight loss was periodically checked (interval, approximately 10 min) until the weight remained constant. At this point, the water from the fluid phase was considered to be extracted entirely. The temperature of the drying oven was 110°C, except for glass samples with expected water concentrations exceeding 6 wt.% H_2O. For these glasses, the oven temperature was between 50°C and 70°C.

The mole fractions of H_2O and CO_2 in the fluid (Table 2) were calculated as follows:

$$X^{f}_{H_2O} = \frac{\left(\frac{m_{H_2O}}{18.02}\right)}{\left(\frac{m_{CO_2}}{44.01} + \frac{m_{H_2O}}{18.02} + \frac{m_{N_2}}{28.01}\right)} \quad (1)$$

$$X^{f}_{CO_2} = \frac{\left(\frac{m_{CO_2}}{44.01}\right)}{\left(\frac{m_{CO_2}}{44.01} + \frac{m_{H_2O}}{18.02} + \frac{m_{N_2}}{28.01}\right)} \quad (2)$$

In these calculations, we take into account that atmospheric N_2 was trapped in the experimental charge during preparation of the capsule. We esti-

mate the resulting mole fraction of N_2 in the fluid phase ($X^f_{N_2}$) to be in the range 0.5–4 mol%. This variation is due to varying melt/fluid ratios and capsule lengths. The estimated $X^f_{N_2}$ are consistent with the $X^f_{N_2}$ determined by gas chromatography on the remaining fluid phase of similar solubility experiments performed with haplogranitic melts (Behrens, unpublished data). Furthermore, minor amounts of CO (< 0.12 mol%) were detected in CO_2-rich fluids. However, as concentrations of additional components are low, we consider the fluid phase as a two-component gas mixture of CO_2 and H_2O.

Using the gravimetric method (described above), the individual weights of CO_2 and N_2 could not be distinguished. Therefore, the enclosed N_2 represents the main source of error in the determination of $X^f_{CO_2}$ and $X^f_{H_2O}$. To account for N_2, we assumed an average $X^f_{N_2}$ of 0.02 ± 0.02 for all experiments, except for experiments with pure water where $X^f_{N_2}$ was negligible (< 0.01). When N_2 and CO_2 are measured together and H_2O is measured independently, the error is larger in $X^f_{CO_2}$ than in $X^f_{H_2O}$. The maximum error on $X^f_{CO_2}$ is given by $X^f_{N_2}$ in the fluid phase. The corresponding error on $X^f_{H_2O}$, resulting from the difference in molar mass between N_2 (28.01 g mol^{-1}) and CO_2 (44.01 g mol^{-1}), is $0.36X^f_{N_2}$. To calculate the errors on $X^f_{CO_2}$ and $X^f_{H_2O}$ given in Table 2, we have taken into account the weighing uncertainty (0.1 and 0.05 mg for CO_2 and H_2O, respectively) and the error induced by atmospheric N_2 (0.02 and 0.007 mol% for CO_2 and H_2O, respectively).

The gravimetric method was found to be accurate for fluid compositions $0.1 < X^f_{H_2O} < 0.9$. However, for extreme CO_2- or H_2O-rich fluids, this method is not suitable because water and CO_2 cannot be separated properly. Therefore, in these cases, we have used mass balance to determine the composition of the fluid phase.

3.2. Density determination

Densities of the rhyolitic glasses were measured by weighing the single glass pieces in air and in water. The principal source of error using this method arises from weighing the sample in water, where problems related to surface creep introduce 0.2 mg uncertainty, estimated by repeated measurements on standards. For the relatively small samples obtained in the solubility experiments (20–40 mg), the resulting error is typically 2% relative. Densities of a total number of 22 hydrous rhyolitic samples including two samples synthesised at 150 MPa were measured. The density data of nine glasses obtained from our solubility experiments are given in Table 3. As already observed by several authors (e.g., Silver et al., 1990; Richet et al., 1996; Schulze et al., 1996; Behrens et al., 1996; Richet and Polian, 1998), the dependence of density on water content can be modelled by a linear equation:

$$\rho = \rho_0 + mC_{\text{water}} \quad (3)$$

where ρ is the density of the hydrated glass, ρ_0, the density of the dry glass, m, a constant, and C_{water}, the total water content (expressed in wt.%). An updated weighted least-square regression was performed for the EDF rhyolitic composition using our 22 samples and data from Withers and Behrens (2000). The density data of Withers and Behrens (2000) are systematically higher than those determined in our study (Fig. 1). This deviation can be explained by the difference in synthesis pressure (Withers and Behrens, 1999. 500 MPa; this study, 150–500 MPa) and sample size (smaller samples and, therefore, higher uncertainty on density determination in our study), and by a possible effect of dissolved CO_2 in the glasses.

Fitting all the data to Eq. (3) we have calculated ρ_0 and m to be 2367.7 (± 15.6) and -14.72 (± 3.50), respectively, for rhyolitic glasses (see Fig. 1). To be internally consistent in this study, the glass densities which need to be known for the determination of volatile concentrations from IR spectra, were all calculated by this density–water content relationship. It is emphasised that the density–water content relationship defined by Withers and Behrens (1999) may adequately predict densities at 500 MPa. However, to calculate densities of rhyolitic glasses produced over a wide pressure range (150–500 MPa), the new relationship is recommended.

3.3. Karl–Fischer titration (KFT)

The water contents of some of the experimental glasses was measured by pyrolysis and subsequent

Table 3
Spectroscopic data

Sample	Measured density (g l^{-1})	Calculated density (g l^{-1})[a]	MIR			NIR				
			Thickness (cm)[b]	A_{2346}	C_{CO_2} (wt.%)	Thickness (cm)	A_{4520}	A_{5230}	C_{OH} (wt.%)	C_{H_2O} (wt.%)
Ech1[c]	–	2325	0.0112 (1)	0.598	0.095 (3)	0.0500	0.128	0.163	1.41 (0.08)	1.52 (0.06)
Ech7[c]	–	2321	0.0111 (3)	0.525	0.084 (4)	0.0493	0.129	0.186	1.44 (0.08)	1.76 (0.06)
Ech6[c]	–	2312	0.0112 (4)	0.414	0.066 (4)	0.0486	0.134	0.237	1.52 (0.09)	2.29 (0.08)
Ech2[c]	–	2310	0.0109 (2)	0.432	0.071 (3)	0.0495	0.138	0.253	1.54 (0.09)	2.40 (0.08)
Ech8[c]	–	2307	0.0111 (3)	0.393	0.063 (3)	0.0492	0.137	0.271	1.54 (0.09)	2.59 (0.09)
Ech9	–	2300	0.0116 (5)	0.304	0.047 (3)	0.0484	0.140	0.308	1.61 (0.09)	3.00 (0.10)
Ech10[c]	2300 (52)	2294	0.0117 (1)	0.190	0.029 (2)	0.0495	0.144	0.356	1.62 (0.09)	3.40 (0.11)
Ech3	–	2281	–	–	–	0.0496	0.142	0.449	1.60 (0.09)	4.31 (0.14)
Ech4	2274 (51)	2280	–	–	–	0.0496	0.147	0.449	1.66 (0.09)	4.31 (0.14)
Ech66	–	2360	0.0077 (7)	0.461	0.105 (14)	0.0810	0.073	0.009	0.49 (0.03)	0.05 (0.02)
Ech65	–	2347	0.0077 (4)	0.465	0.106 (9)	0.0814	0.148	0.074	0.99 (0.05)	0.42 (0.02)
Ech64	–	2337	0.0095 (4)	0.537	0.100 (7)	0.0810	0.179	0.147	1.21 (0.07)	0.84 (0.03)
Ech63	–	2331	0.0096 (1)	0.481	0.089 (3)	0.0805	0.194	0.198	1.32 (0.07)	1.14 (0.04)
Ech62	–	2326	0.0088 (2)	0.404	0.081 (4)	0.0810	0.205	0.253	1.39 (0.08)	1.46 (0.06)
Ech17	–	2316	0.0117 (2)	0.441	0.067 (3)	0.0500	0.139	0.213	1.53 (0.09)	2.00 (0.07)
Ech18	2278 (51)	2311	0.0121 (3)	0.427	0.063 (3)	0.0504	0.142	0.248	1.56 (0.09)	2.31 (0.08)
Ech19	2275 (51)	2303	0.0123 (2)	0.321	0.047 (2)	0.0492	0.145	0.285	1.64 (0.09)	2.73 (0.09)
Ech20	2273 (51)	2299	0.0119 (3)	0.262	0.040 (2)	0.0489	0.147	0.311	1.67 (0.09)	3.00 (0.10)
Ech21	–	2286	–	–	–	0.0489	0.151	0.396	1.73 (0.09)	3.85 (0.13)
Ech37	2291 (52)	2291	0.0053 (1)	0.598	0.203 (7)	0.0496	0.146	0.371	1.64 (0.09)	3.54 (0.12)
Ech38	2274 (51)	2289	0.0051 (1)	0.592	0.209 (8)	0.0495	0.145	0.384	1.64 (0.09)	3.68 (0.12)
Ech39	2229 (50)	2272	0.0047 (2)	0.430	0.166 (10)	0.0494	0.145	0.500	1.65 (0.09)	4.84 (0.16)
EDF (1)	–	2223	–	–	–	–	–	–	–	–
Ech75	–	2360	0.0036 (2)	0.566	0.275 (29)	0.0975	0.082	0.010	0.45 (0.03)	0.05 (0.01)
Ech74	–	2351	0.0044 (1)	0.682	0.272 (15)	0.0962	0.153	0.059	0.86 (0.05)	0.28 (0.02)
Ech73	–	2348	0.0056 (3)	0.898	0.282 (22)	0.0956	0.168	0.083	0.95 (0.05)	0.40 (0.02)
Ech72	–	2341	0.0063 (2)	0.903	0.253 (10)	0.0957	0.198	0.143	1.13 (0.06)	0.69 (0.03)
Ech59	–	2332	0.0064 (2)	0.965	0.267 (10)	0.0579	0.139	0.141	1.32 (0.07)	1.13 (0.04)
Ech71	–	2336	0.0060 (2)	0.901	0.266 (13)	0.0953	0.215	0.193	1.24 (0.07)	0.94 (0.03)
Ech58	–	2319	0.0058 (2)	0.837	0.257 (13)	0.0586	0.155	0.229	1.46 (0.08)	1.83 (0.06)
Ech57	–	2310	0.0051 (5)	0.715	0.251 (25)	0.0589	0.162	0.299	1.52 (0.08)	2.39 (0.08)
Ech11	–	2297	0.0052 (3)	0.675	0.233 (15)	–	–	–	–	–
Ech22[d]	–	2293	0.0058 (4)	0.747	0.232 (18)	0.0511	0.147	0.377	1.60 (0.09)	3.49 (0.12)
Ech56	–	2291	0.0050 (1)	0.609	0.220 (8)	0.0591	0.172	0.448	1.62 (0.09)	3.59 (0.12)
Ech61	–	2272	0.0062 (3)	0.604	0.177 (9)	0.0601	0.176	0.614	1.65 (0.09)	4.88 (0.16)
Ech24[d]	–	2269	0.0054 (3)	0.569	0.192 (13)	0.0502	0.149	0.528	1.67 (0.09)	5.03 (0.17)
Ech41	2216 (50)	2264	0.0051 (5)	0.466	0.167 (19)	0.0501	0.147	0.562	1.66 (0.09)	5.38 (0.18)
Ech36	–	2247	0.0050 (2)	0.257	0.094 (7)	0.0500	0.141	0.682	1.60 (0.09)	6.59 (0.22)
Ech49	–	2212	–	–	–	0.0249	0.080	0.443	1.86 (0.12)	8.73 (0.31)

Concentrations on C_{OH} and C_{H_2O} are given in wt.% H_2O. Total water determined from NIR is the sum of C_{OH} and C_{H_2O}. See text for details about error calculations.

[a] Densities are calculated using Eq. (3). See text for more details.

[b] Thicknesses are calculated using Eq. (5). Sample thickness and peak heights are average values derived from 3 to 9 spectra measured in different areas of the samples, including rim and core. See text for more details.

[c] Quenched glass contains aggregates of metallic silver.

[d] Sample with bubbles (< 10 vol.%).

KFT. The apparatus and analytical technique are described in detail by Behrens et al. (1996). One or two chips of glass (15–30 mg) are heated to 1300°C in order to extract the dissolved water. The released

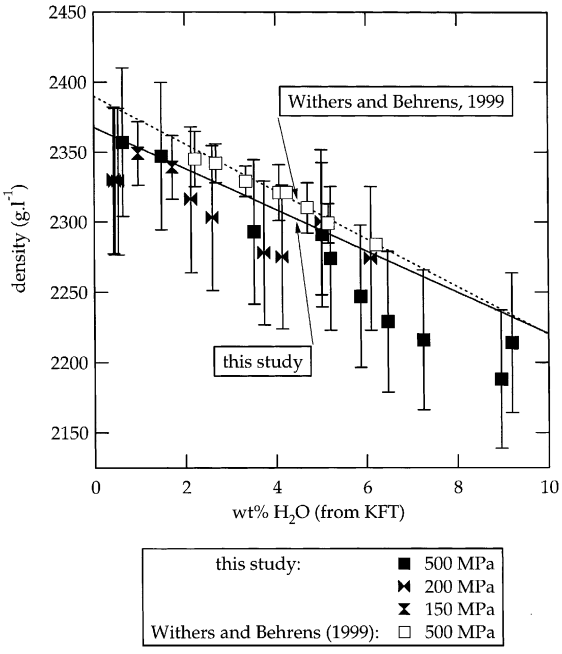

Fig. 1. Density–water content for rhyolitic glasses. The linear fit of Withers and Behrens (1999) is based on data from glasses synthesised at 500 MPa only (dashed line). The new fit (solid line) combines the data from Withers and Behrens (1999) and from this study (data obtained at 150 200 and 500 MPa).

water is transported by an Ar flux to a titration cell and analysed by a coulometric method (KFT). Uncertainties in measured water contents were calculated on the basis of ± 0.02 μg s^{-1} uncertainty in titration rate (Behrens et al., 1996), also taking into account a residual (unextracted) water content of 0.10 ± 0.05 wt.% (Behrens, 1995).

3.4. IR spectroscopy

3.4.1. Sample preparation and analysis conditions

Small pieces were cut from the middle of the sample and doubly polished down to a thickness of either 480–1000 μm for NIR or 35–125 μm for MIR spectroscopy. The thickness of each glass chip was measured using a digital micrometer. An estimate of ± 0.0003 cm was assumed for the uncertainty in thickness. The thicknesses of the polished sections were in part difficult to measure with the micrometer due to bending of the glass. Therefore, we have used the interference fringes in the IR spectra for thickness determination of the samples investigated with MIR spectroscopy (Fig. 2). This method has the advantage that peak intensities and thicknesses are measured exactly at the same position of the sample.

If the measurement beam is oriented perpendicular to the glass chip, the wave length λ of the interference fringes is given by:

$$\lambda = \frac{1}{2\,dn} \tag{4}$$

where d is the thickness and n the refractive index. This equation cannot be applied directly for thickness determination because (1) the refractive indexes of the rhyolitic glasses are not exactly known in the MIR (only a value of $1.48 < n < 1.51$ in the visible is given by Tröger, 1959) and (2) the beam of the IR microscope is focused at the sample position. Thus, the factor, which links the thickness and the inverse of the wavelength, has to be determined experimentally. Using a set of 53 samples for which we have measured interference fringes in the range 2070–2270 cm^{-1}, we found a linear relationship of d and $1/\lambda$ (Fig. 3). By linear regression we obtained:

$$d = \frac{0.3176(\pm 0.0024)}{\lambda} \tag{5}$$

Throughout our study, Eq. (5) was used for determination of thicknesses of MIR sections.

Spectra were collected with a Bruker IFS 88 FTIR spectrometer coupled with an IR microscope A590. The spot size used in our measurements was approximately 80–100 μm (Nowak and Behrens, 1997). Operation conditions were: light source — W lamp and Glowbar for NIR and MIR, respectively; beamsplitter — CaF_2 and KBr, for NIR and MIR, respectively; detector — narrow band MCT with NIR equipment (range 600–10000 cm^{-1}); number of accumulated scans — 100. For CO_2 acquisition, increasing the number of scans up to 600 scans was tested with no improvement of the quality of the spectra (no attenuation of scattering). In order to lower atmospheric effects, especially during MIR analysis, the sample stage of the IR microscope was isolated from the atmosphere in a chamber. Both the whole microscope and the chamber were purged

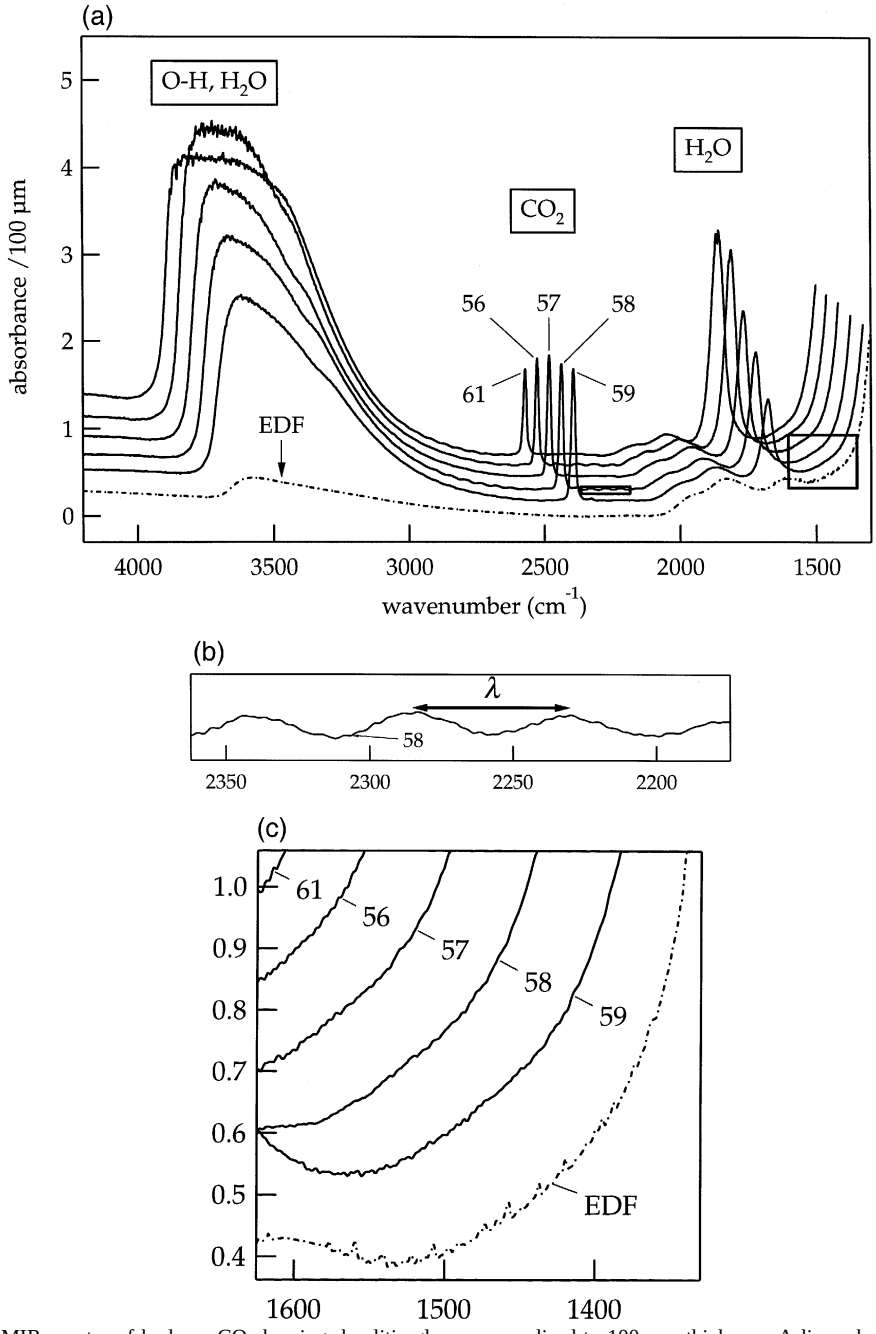

Fig. 2. (a) Typical MIR spectra of hydrous CO_2-bearing rhyolitic glasses normalised to 100-μm thickness. A linear base line fitted to the feet of the CO_2 peak was subtracted. A spectrum from natural EDF is shown for comparison (dashed line). For clarity spectra of experimental glasses are plotted with x/y offsets. Numbers refer to the experimental runs in Table 2 and Table 3. (b) Detail showing the interference fringes in the domain where sample thicknesses were determined. (c) Detail showing the 1325–1625 cm^{-1} are where carbonate doublets were observed in glasses of other compositions. No evidence of carbonate could be found in any of the rhylolitic glasses.

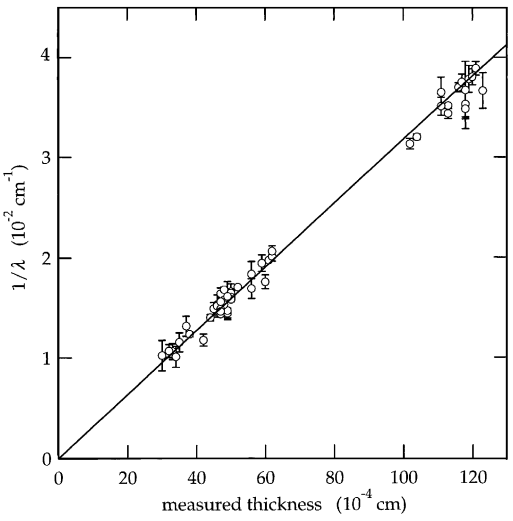

Fig. 3. Calibration curve of sample thickness as a function of the inverse wavelengths of interference fringes.

with dry air. Furthermore, a new background was taken before each sample measurement.

3.4.2. NIR spectroscopic determination of water contents

The concentrations of H_2O and OH were determined from the heights (see Table 3) of the baseline corrected absorption bands at 5230 and at 4520 cm^{-1}, which are attributed to the combination stretching + bending mode of molecular H_2O and combination stretching + bending mode of OH groups (Scholze, 1960; Bartholomew et al., 1980; Stolper, 1982) by using the Lambert–Beer law. We used an appropriate automated two linear tangent baseline subtraction method (described in detail in Withers and Behrens, 1999) to increase the reliability of the method. Linear molar absorption coefficients of 1.41 and 1.66 l cm^{-1} mol^{-1} for the 4520 and 5230 cm^{-1} bands, respectively, are used to calculate the total water contents (Withers and Behrens, 1999).

3.4.3. MIR spectroscopic determination of CO_2 contents

The concentrations of carbon species were determined from the heights (see Table 3) of the baseline corrected MIR absorption band at 2346 cm^{-1} assigned to the fundamental ν_3 vibration of CO_2 molecules (Fig. 2a). No carbonate species was detected in any of the rhyolitic glasses (Fig. 2c). This is consistent with former studies on CO_2 solubility in rhyolite (cf. Fogel and Rutherford, 1990; Blank et al., 1993). The height of the 2346 cm^{-1} peak was determined using an automated linear tangent baseline subtraction method. We used the linear molar absorption coefficient of 1066 l cm^{-1} mol^{-1} determined by Blank (1993). A major problem in our measurements has been that the IR beam could not be isolated completely from the atmosphere. Thus, the CO_2 content of the air in the beam path may vary during the measurements. To quantify this variation, we have compared 92 spectra collected without sample. These spectra were recorded in two ways over a period of several days: (1) series of around 10 spectra without sample were successively recorded without opening the sample chamber of the IR microscope; (2) one or several spectra without sample were directly collected after the IR measurements performed on each glass sample. The variation in peak intensity was found to be random, suggesting rapid changes of atmospheric CO_2 concentrations with time. An average peak intensity of the atmospheric CO_2 band at 2349 cm^{-1} corresponding to 0.014 ± 0.0010 absorbance unit was determined for our measurement conditions. This value, which corresponds to an equivalent CO_2 content of 25 ppm for a 100-μm thick sample, is considered to be the precision of CO_2 absorbance measurement.

4. Results and discussion

4.1. Quenched products

The solid-run products consist of clear, weakly coloured to colourless glasses (except sample 11, which contains up to 2 wt.% Ag), which were mostly bubble and crystal free. Bubbles are only observed in two samples (Ech22 and Ech24) synthesised in an experiment, which was started twice (due to failure of the furnace), and are small and homogeneously distributed. Few crystals were observed at 800°C and 200 MPa for $X^f_{H_2O} < 0.35$ (Table 2). The crystals were too small to be analysed by microprobe, but no noticeable change in the melt composition was observed. The composition of each glass was checked

by electron microprobe for possible changes during the experiments. Only a loss of iron in experiments performed with Pt capsules was observed, especially at the rims of the glasses. However, as the iron content in the starting glass is low, we assume that the loss of iron to the capsule has no significant effect on volatile solubilities.

The H_2O and CO_2 contents of glasses are given in Table 3. All samples analysed by IR spectroscopy show a homogeneous distribution of water and CO_2 with no detectable difference between rim and core of glasses within analytical error. An exception is sample Ech75 in which CO_2 concentration varied between 0.235 (core) and 0.293 wt.% (rim). In this run, the fluid was extremely water poor, and we assume that the run duration was insufficient to homogenise the melt. This interpretation is supported by diffusion data (Watson, 1994; Zhang and Behrens, 2000) showing a strong decrease of CO_2 and H_2O diffusivity with decreasing water content in the melt. The CO_2 solubility of Ech75 given in Table 3 corresponds to the average of the five highest solubilities measured at the rim of the sample. This value is assumed to be close to the equilibrium solubility.

It can be noted that for water contents > 7 wt.%, the NIR spectroscopy method tends to underestimate water contents as shown by comparison to the KFT data (maximum difference, 0.77 wt.%, Ech36). A possible explanation is that some water was lost during sample preparation (before polishing, samples are heated up to 60–70°C). This interpretation is supported by the results obtained for the most water-rich sample (Ech49), which was not polished, and for which the NIR and KFT values are almost within the error bar. Therefore, we decided to consider the KFT data as representative for the water solubility in water rich samples (Ech36, Ech49).

4.2. H_2O solubility

Fluid compositions and the corresponding water and CO_2 contents of the quenched glasses are presented in Tables 2 and 3, respectively. At both 200 and 500 MPa, a square root dependence of water solubility on $X^f_{H_2O}$ is observed at low $X^f_{H_2O}$ (Fig. 4). At 200 MPa, a linear function between water solubility and $X^f_{H_2O}$ allows to model all data within uncertainty for $0.25 < X^f_{H_2O} < 1$. At 500 MPa, the water solubility shows a non linear dependence on $X^f_{H_2O}$ in the whole $X^f_{H_2O}$ range. The 500 MPa data indicate a point of inflexion at around $X^f_{H_2O} \sim 0.5$.

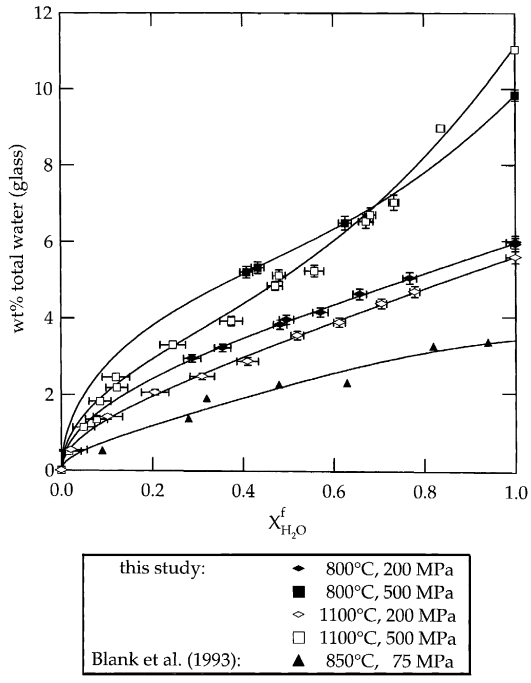

Fig. 4. Relationship between the mole fraction of H_2O in the fluid phase and the concentration of total water dissolved in the melt of various temperatures and pressures. Solid lines are the fits of the data used for the empirical model developed in this study. Data from Blank et al. (1993) at 75 MPa are shown for comparison.

The temperature dependence of water solubility is different at 200 and 500 MPa. At 200 MPa, the water solubility decreases with increasing temperature, regardless of the composition of the fluid phase. The water solubility variation as a function of temperature is constant in the investigated range of $X^f_{H_2O}$ ($0.25 < X^f_{H_2O} < 1$) and corresponds to -0.16 wt.% H_2O per 100°C. This value is similar to that observed for a haplogranitic composition at $X^f_{H_2O} = 1$ (Holtz et al., 1992). At 500 MPa, the temperature dependence of water solubility changes from positive for $X^f_{H_2O} > 0.75$ to negative for $X^f_{H_2O} < 0.75$. Water solubility is found to be independent of temperature at a water content of approximately 7 wt.%.

Behrens et al. (2000) showed that the pressure at which water solubility at $X^f_{H_2O} = 1$ is independent

on temperature depends on the melt composition and especially on the aluminium charge balancing cation (compare also results from Paillat et al., 1992; Holtz et al., 1995). For a subaluminous composition with approximately the same Na/K ratio as EDF, the water solubility at $X^f_{H_2O} = 1$ is independent on temperature at approximately 350 MPa (composition AOQ, Holtz et al., 1995), which corresponds to a water content of about 8 wt.%. This amount of water is close to the water content at which water solubility in rhyolitic melts coexisting with mixed fluids is independent on temperature at 500 MPa (7 wt.%). The small difference may be attributed to compositional differences of the melts and experimental uncertainties. Thus, for a given composition, the temperature dependence of water solubility does not depend on total pressure but on the prevailing f_{H_2O}.

4.3. CO_2 solubility

CO_2 solubility increases with increasing $X^f_{CO_2}$ in the fluid phase (Fig. 5) and increasing pressure. The variation of CO_2 solubility with $X^f_{CO_2}$ is non-linear. The deviation from linearity, which increases with pressure and is especially pronounced at 500 MPa. Extrapolating our data set to $X^f_{CO_2} = 1$, the maximum solubilities are 0.11 ± 0.01 and 0.28 ± 0.03 wt.% at 1100°C and 200 and 500 MPa, respectively. At 800°C, the melts are partially crystallised when using CO_2-rich fluids ($X^f_{CO_2} > 0.65$ at 200 MPa, $X^f_{CO_2} > 0.5$ at 500 MPa) and prediction of the solubility of pure CO_2 is not realistic.

To compare our CO_2 solubility data with those from Fogel and Rutherford (1990), we have interpolated their data and have applied a correction to take the difference in absorption coefficient into account (Fogel and Rutherford used absorption coefficients for albitic glasses from Fine and Stolper, 1985). The so obtained CO_2 solubility for $X^f_{CO_2} \approx 1$ at 1100°C, 200 and 500 MPa are 15–20% lower than our extrapolated data (Figs. 5 and 6). The differences may result from experimental uncertainties in the study of Fogel and Rutherford (1990). Fogel and Rutherford (1990) determined the solubility of CO_2 from diffusion profiles. However, gradients of CO_2 and/or H_2O were observed even in long-term experiments,

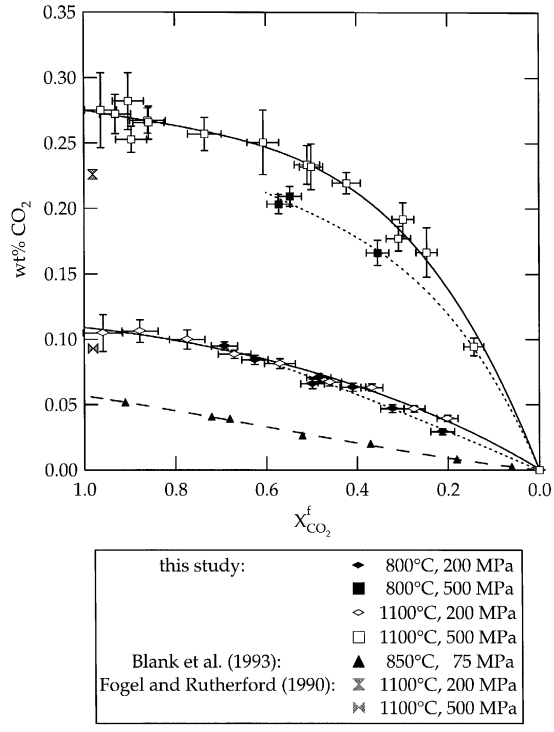

Fig. 5. Relationship between the mole fraction of CO_2 in the fluid phase and the concentration of CO_2 in the melt at various pressures and temperatures. Data from Fogel and Rutherfold (1990) and Blank et al. (1993) are shown for comparison. Solid lines represent trends at 1100°C and dotted lines at 800°C. The dashed line show the trend of the data obtained at 850°C and 75 MPa by Blank et al. (1993).

and extrapolating the CO_2 diffusion profiles to determine CO_2 solubility may underestimate the equilibrium solubility. Furthermore, the composition of the fluid was not analysed. As noted by the authors, the fluid contained minor amounts of H_2O and possibly up to 30 mol% CO. Assuming an $X^f_{CO_2}$ of 0.7, the solubility data of Fogel and Rutherford are in a good agreement with our data.

Within the uncertainty of the data, no obvious effect of temperature on CO_2 solubility is observed at 200 MPa (Fig. 5). However, the data indicate a slight positive temperature dependence on CO_2 solubility at 500 MPa (for $X^f_{CO_2} < 0.5$). It is interesting to note that this effect of temperature on CO_2 solubility for $X^f_{CO_2} < 0.5$ differs from that observed by Fogel and Rutherford (1990) at $X^f_{CO_2} = 1$. These authors found that an increase of temperature from

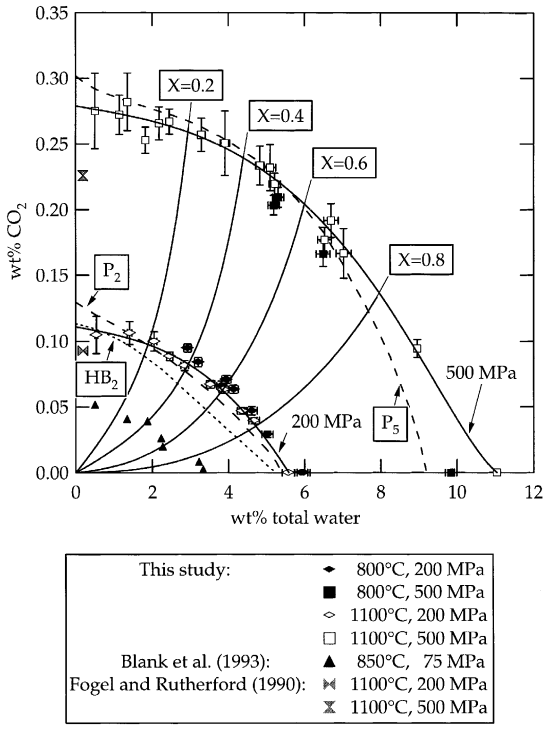

Fig. 6. Relationship between total water and CO_2 contents dissolved in rhyolitic melt at various pressures and temperatures. Data from Fogel and Rutherfold (1990) and Blank et al. (1993) are shown for comparison. The solid lines are isotherms fitted to experimental data at 1100°C. *X* values correspond to the mole fraction of water in the fluid phase. The dotted line labelled HB_2 shows the predictions of Holloway and Blank (1994) at 900°C (200 MPa), and the dashed lines labelled P_2 and P_5 the predictions of Papale (1999) at 900°C (200 and 500 MPa), respectively.

950°C to 1150°C produces a decrease in the CO_2 solubility both at 200 and 500 MPa.

4.4. Comparison with calculations

Fig. 6 shows the experimental data for H_2O and CO_2 solubility in rhyolitic melts coexisting with H_2O–CO_2 fluids and the predicted values using the thermodynamic models of Holloway and Blank (1994) and Papale (1999).

The model of Holloway and Blank (1994) is based on the water solubility model of Burnham (1979) and the CO_2 solubility models of Spera and Bergman (1980) and Stolper et al. (1987). The calculated data for rhyolitic melts at 200 MPa and 850°C are slightly lower than the water and CO_2 solubilities determined experimentally at 200 MPa and 800°C (approximately 8–10% relative, for water solubility). The temperature dependence of volatile solubility is too small to account for this deviation. A possible explanation is the use of the model of Burnham (1979), which underestimates the water solubility, especially at high pressure (Holtz et al., 1995). Thus, the model of Holloway and Blank (1994) probably allows the prediction of H_2O and CO_2 solubilities with a precision better than $\pm 10\%$ relative below 200 MPa. More significant deviations are observed if the model is used at higher pressures. At 500 MPa, the calculated and experimentally determined water solubilities for $X^f_{H_2O} = 1$ differ by 15% relative at 800°C. These differences are more pronounced at higher temperatures, because the strong positive temperature dependence of water solubility at 500 MPa is not predicted by the model of Burnham (1979).

The model of Papale (1999) reproduces experimental data at 200 and 500 MPa much better than the model of Holloway and Blank (1994) does. At 200 MPa, the predicted and experimentally determined values agree within experimental error. At higher pressure, however, the model of Papale tends to underestimate the water solubility. For example, at 500 MPa, our data for pure H_2O solubility interpolated to 900°C are 1 wt.% higher than the prediction of Papale (1999). It is interesting to note that despite the relatively small CO_2 solubility database of the model, the predictions of CO_2 solubility are close to our experimental data.

4.5. Empirical model for water solubility between 75 and 500 MPa

In order to improve the prediction of water solubility as a function of the fluid phase composition, we have developed an empirical model based on our data set and that of Blank et al. (1993). At a given temperature and pressure, the data plotted in Fig. 4 can be fitted adequately by an equation of the form:

$$C_{\text{water}}\ (\text{wt.\%}) = Ax^2 + Bx^{2.5} + Cx^{0.5} \qquad (6)$$

where C_{water} is the total water content of the glass, *A*, *B* and *C* are empirical coefficients and *x* is the composition of the fluid phase in equilibrium with the melt ($x = X^f_{H_2O}$). The curves in Fig. 4 result from the fit of each data set to Eq. (6).

Table 4
Fit parameters of Eq. (7)

	$A_{(P,T)}$		$B_{(P,T)}$		$C_{(P,T)}$	
	a_A	b_A	a_B	b_B	a_C	b_C
$\alpha_{i,j}$	-14.749	2.7296×10^{-2}	12.615	-2.3041×10^{-2}	5.4181	-6.11323×10^{-3}
$\beta_{i,j}$	7.67×10^{-2}	-1.3688×10^{-4}	-6.3322×10^{-2}	1.1396×10^{-4}	1.2838×10^{-2}	2.0095×10^{-5}
$\gamma_{i,j}$	-2.0868×10^{-4}	2.5324×10^{-7}	1.5411×10^{-4}	-1.747×10^{-7}	1.4632×10^{-5}	-4.8208×10^{-8}

At low water fugacity, the third term in Eq. (6) is dominating and water solubility varies with the square root of $X^{f}_{H_2O}$. This is consistent with water speciation data, which demonstrate that water is preferentially incorporated in silicate melts as OH groups at low water contents (Nowak and Behrens, 1995; Sowerby and Keppler, 1999). At high water fugacity, the first and second term in Eq. (6) becomes increasingly important. This behaviour may be related to increasing amounts of molecular H_2O with increasing water content.

To model the temperature dependence, a linear variation of water solubility as a function of temperature was assumed. Such a temperature dependence has been observed experimentally over a wide temperature range for $P < 500$ MPa. As the data from Blank et al. (1993) are only given at 850°C, their data were extrapolated to 1100°C using the temperature dependence of water solubility found at 200 MPa (Holtz et al., 1995 have shown that the temperature dependence of water solubility is almost identical between 50 and 200 MPa, at least for $X^{f}_{H_2O} = 1$). The pressure dependence has been modelled assuming a third order polynomial dependence of water solubility on pressure. The Eq. (6) can be rewritten as:

$$C_{\text{water}}(\text{wt.\%}) = A_{P,T}\,x^2 + B_{P,T}\,x^{2.5} + C_{P,T}\,x^{0.5} \quad (7)$$

where

$$A_{P,T} = \left(\alpha_{a_A} + \beta_{a_A}P + \gamma_{a_A}P^2\right) + \left(\alpha_{b_A} + \beta_{b_A}P + \gamma_{b_A}P^2\right)T \quad (8a)$$

$$B_{P,T} = \left(\alpha_{a_B} + \beta_{a_B}P + \gamma_{a_B}P^2\right) + \left(\alpha_{b_B} + \beta_{b_B}P + \gamma_{b_B}P^2\right)T \quad (8b)$$

$$C_{P,T} = \left(\alpha_{a_C} + \beta_{a_C}P + \gamma_{a_C}P^2\right) + \left(\alpha_{b_C} + \beta_{b_C}P + \gamma_{b_C}P^2\right)T \quad (8c)$$

The values of the empirical coefficients $\alpha_{i,j}$, $\beta_{i,j}$, $\gamma_{i,j}$ are given in Table 4. P is given in MPa and T in °C.

The empirical model reproduces our data within ±2.5% relative, except at 500 MPa, 1100°C (±5% relative). We have tested the validity of the model from experiments performed in synthetic and natural rhyolitic compositions obtained for $X^{f}_{H_2O} = 1$ in the pressure range 75–500 MPa and temperature range

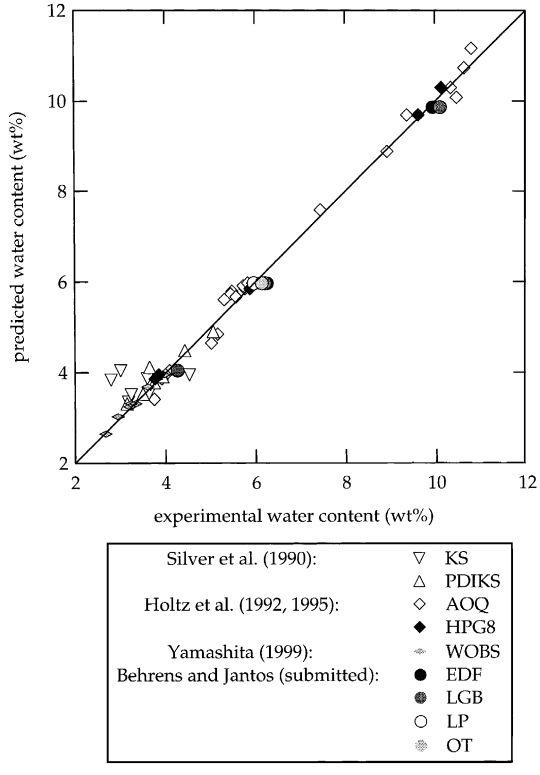

Fig. 7. Comparison of water solubilities calculated from the empirical model given by Eq. (7) with experimental water solubility data in the pressure and temperature range 75–500 MPa and 800–1100°C. The model reproduces most of water solubility data within ±5.5%. All compositions represents synthetic or natural rhyolites (see text).

800–1100°C. The data sets that have been considered are from Silver et al. (1990, compositions PDIKS, KS), Holtz et al. (1992, 1995, compositions AOQ, HPG8), Yamashita (1999, composition WOBS) and Behrens and Jantos (submitted, compositions EDF, LGB, OT, LP). All the compositions are quartzofeldspathic or close to subaluminous rhyolitic compositions. The empirical model reproduces 48 of 53 experimental water solubility data within ±5.5% relative. Two experiments are reproduced within ±7.5% relative (AOQ) and three are within ±12.5–36% relative (PDIKS, KS). The comparison of calculated and experimentally determined water solubilities for $X^{f}_{H_2O} = 1$ is shown in Fig. 7.

Although our model is empirical, it is a useful tool to predict water solubilities in rhyolitic melts in geologically relevant conditions at various $X^{f}_{H_2O}$ because it has high precision and can be run easily. It is emphasised that the model is valid only between 75 and 500 MPa and 800°C and 1100°C. As polynomials are used in the model, an extrapolation out of this range results in a large error (for example, the calculated water solubility at 800°C and 800 MPa is 20% lower than the experimental solubility determined for haplogranitic melts by Holtz et al., 1995).

Acknowledgements

This study has been supported by the European Community (TMR project ERBFMRX-CT96-0063 G) and the German DFG (project HO 1337/3-1). The authors are grateful to O. Diedrich, A.C. Withers, B. Clemente, C. Rüscher for technical assistance and to B. Schmidt and J. Sowerby for constructive comments.

References

Bagdassarov, N.S., Dingwell, D.B., 1993. Frequency-dependent rheology of vesicular rhyolite. J. Geophys. Res. 98, 6477–6487.

Bartholomew, R.F., Butler, B.L., Hoover, H.L., Wu, C.K., 1980. Infrared spectra of a water-containing glass. J. Am. Ceram. Soc. 63, 481–485.

Becker, A., Holtz, F., Johannes, W., 1998. Liquid temperatures and phase compositions in the system Qz–Ab–Or at 5 kbar and very low water activities. Contrib. Miner. Petrol. 130, 213–224.

Behrens, H., 1995. Determination of water solubilities in high-viscosity melts: an experimental study of $NaAlSi_3O_8$ and $KAlSi_3O_8$ melts. Eur. J. Miner. 7, 905–920.

Behrens, H., Jantos, N., submitted. The effect of anhydrous composition on water solubility in granitic melts. Am. Mineral., submitted for publication.

Behrens, H., Schmidt, M.O., 1998. Infrared spectroscopy of hydrous silicic glasses at temperatures up to 600°C and implications for the incorporation and dynamics of water in glasses. Neues Jahrb. Mineral., Abh. 172, 203–226.

Behrens, H., Romano, C., Nowak, M., Holtz, F., Dingwell, D.B., 1996. Near-infrared spectroscopic determination of water species in glasses of the system $MAlSi_3O_8$ (M = Li, Na, K): an interlaboratory study. Chem. Geol. 128, 41–63.

Behrens, H., Meyer, M., Holtz, F., Benne, D., Nowak, M., 2000. The effect of alkali ionic radius, temperature, and pressure on the solubility of water in $MAlSi_3O_8$ melts (M = Li, Na, K, Rb). Chem. Geol., in press.

Blank, J.G., 1993. An experimental investigation of the behaviour of carbon dioxide in rhyolitic melt. PhD. dissertation, California Institute of Technology, Pasadena, CA.

Blank, J.G., Brooker, R.A., 1994. Experimental studies of carbon dioxide in silicate melts: solubility, speciation and stable isotope behavior. In: Carroll, M.R., Holloway, J.R. (Eds.), Volatiles in Magmas. Reviews in Mineralogy 30. Mineralogical Society of America, Washington DC, pp. 157–186.

Blank, J.G., Stolper, E.M., Carroll, M.R., 1993. Solubility of carbon dioxide and water in rhyolitic melt at 850°C and 750 bars. Earth Planet Sci. Lett. 119, 27–36.

Burnham, C.W., 1979. The importance of volatile constituents. In: Yoder, H.S. (Ed.), The Evolution of the Igneous Rocks. Princeton Univ. Press, Princeton, NJ, pp. 439–482.

Dingwell, D.B., Hess, K.-U., Romano, C., 1998. Viscosity data for hydrous peraluminous granitic melts: comparison with a metaluminous model. Am. Miner. 83, 236–239.

Fine, G., Stolper, E., 1985. The speciation of carbon dioxide in sodium aluminosilicate glasses. Contrib. Miner. Petrol. 91, 105–121.

Fogel, R.A., Rutherford, M.J., 1990. The solubility of carbon dioxide in rhyolitic melts: a quantitative FTIR study. Am. Mineral. 75, 1311–1326.

Hess, K.-U., Dingwell, D.B., Webb, S.L., 1995. The influence of excess alkalies on the viscosity of a haplogranitic melt. Am. Mineral. 80, 297–304.

Holloway, J.R., Blank, J.G., 1994. Application of experimental results to C–H–O species in natural melts. In: Carroll, M.R., Holloway, J.R. (Eds.), Volatiles in Magmas. Reviews in Mineralogy 30. Mineralogical Society of America, Washington DC, pp. 187–230.

Holtz, F., Behrens, H., Dingwell, D.B., Taylor, R.P., 1992. Water solubility in melts of haplogranitic composition at 2 kbar. Chem. Geol. 96, 289–302.

Holtz, F., Behrens, H., Dingwell, D.B., Johannes, W., 1995. H_2O solubility in haplogranitic melts: compositional, pressure and temperature dependence. Am. Mineral. 80, 94–108.

Ihinger, P.D., Hervig, R.L., McMillan, P.F., 1994. Analytical methods for volatiles in glasses. In: Carroll, M.R., Holloway,

J.R. (Eds.), Volatiles in Magmas. Reviews in Mineralogy 30. Mineralogical Society of America, Washington DC, pp. 67–121.

Kadik, A.A., Lukanin, O.A., Lebedev, Y.B., Korovushkina, E.Y., 1972. Solubility of H_2O and CO_2 in granite and basalt melts at high pressures. Geochem. Int. 9, 1041–1050.

Kohn, S.C., 2000. The dissolution mechanisms of water in silicate melts: a synthesis of recent data. Mineral. Mag. 64, 389–408.

McMillan, P., 1994. Water solubility and speciation models. In: Carroll, M.R., Holloway, J.R. (Eds.), Volatiles in Magmas. Reviews in Mineralogy 30. Mineralogical Society of America, Washington DC, pp. 131–156.

Nowak, M., Behrens, H., 1995. The speciation of water in haplogranitic glasses and melts determined by in situ near-infrared spectroscopy. Geochim. Cosmochim. Acta 59, 3445–3450.

Nowak, M., Behrens, H., 1997. An experimental investigation on diffusion of water in haplogranitic melts. Contrib. Miner. Petrol. 126, 365–376.

Paillat, O., Elphick, S.C., Brown, W.L., 1992. The solubility of water in $NaAlSi_3O_8$ melts: a re-examination of $Ab–H_2O$ phase relationships and critical behaviour at high pressure. Contrib. Miner. Petrol. 112, 490–500.

Papale, P., 1999. Modeling of the solubility of a two-component H_2O+CO_2 fluid in silicate liquids. Am. Mineral. 84, 477–492.

Richet, P., Polian, A., 1998. Water as a dense, icelike component of silicate glasses. Science 281, 396–398.

Richet, P., Lejeune, A.M., Holtz, F., Roux, J., 1996. Water and the viscosity of andesite melts. Chem. Geol. 128, 185–197.

Schmidt, B.C., Behrens, H., Tamic, N., Holtz, F., Pichavant, M., 1998. Water solubility in haplogranitic melts coexisting with $H_2O–H_2$ and $H_2O–CO_2$ fluids. 8th V.M. Goldschmidt Conference (abstract). Miner. Mag. 62A, 1343–1344.

Schmidt, B.C., Holtz, F., Pichavant, M., 1999. Water solubility in haplogranitic melts coexisting with $H_2O–H_2$ fluids. Contrib. Miner. Petrol. 136, 213–224.

Scholze, H., 1960. Zur Frage der unterscheidung zwischen H_2O–molekeln und OH-gruppen in gläsern und mineralen. Naturwissenschaften 47, 226–227.

Schulze, F., Behrens, H., Holtz, F., Roux, J., Johannes, W., 1996. The influence of water on the viscosity of a haplogranitic melt. Am. Mineral. 81, 1155–1165.

Silver, L.A., Ihinger, P.D., Stolper, E., 1990. The influence of bulk composition on the speciation of water in silicate glasses. Contrib. Miner. Petrol. 104, 142–162.

Sowerby, J.R., Keppler, H., 1999. Water speciation in rhyolitic melt determined by in-situ infrared spectroscopy. Am. Mineral. 84, 1843–1849.

Spera, F.J., Bergman, S.C., 1980. Carbon dioxide in igneous petrogenesis: I. Aspects of the dissolution of CO_2 in silicate liquids. Contrib. Miner. Petrol. 74, 55–66.

Stevenson, R.J., Dingwell, D.B., Webb, S.L., Bagdassarov, N.S., 1995. The equivalence of enthalpy and shear stress relaxation in rhyolitic obsidians and quantification of the liquid–glass transition in volcanic processes. J. Volcanol. Geotherm. Res. 68, 297–306.

Stolper, E., 1982. Water in silicate glasses: an infrared spectroscopic study. Contrib. Miner. Petrol. 81, 1–17.

Stolper, E.M., Fine, G.J., Johnson, T., Newman, S., 1987. The solubility of carbon dioxide in albitic melt. Am. Mineral. 72, 1071–1085.

Taylor, J.R., Wall, V.J., Pownceby, M.I., 1992. The calibration and application of accurate redox sensors. Am. Mineral. 77, 284–295.

Tröger, W.E., 1959. Optische bestimmung der gesteinsbildenden minerale: teil 1, bestimmungstabellen. E. Schweizerbart'sche Verlagsbuchhandlung, Stuttgart.

Watson, E.B., 1994. Diffusion in volatile-bearing magmas. In: Carroll, M.R., Holloway, J.R. (Eds.), Volatiles in Magmas. Reviews in Mineralogy 30. Mineralogical Society of America, Washington DC, pp. 371–411.

Wilke, M., Behrens, H., 1999. The dependence of partitioning of Fe and Eu between plagioclase and hydrous tonalitic melts on oxygen fugacity. Contrib. Miner. Petrol. 137, 102–114.

Withers, A.C., Behrens, H., 2000. Temperature induced changes in the NIR spectra of hydrous albitic and rhyolitic glasses: implications for hydrous species reaction. Phys. Chem. Mineral. 27, 119–132.

Wyllie, P.J., Tuttle, O.F., 1959. Effect of carbon dioxide on the melting of granite and feldspars. Am. J. Sci. 257, 548–655.

Yamashita, S., 1999. Experimental study of the effect of temperature on water solubility in natural rhyolitic melt to 100 MPa. J. Petrol. 40, 1497–1507.

Zhang, Y., 1999. H_2O in rhyolitic glasses and melts: measurement, speciation, solubility, and diffusion. Rev. Geophys. 37, 493–516.

Zhang, Y., Behrens, H., 2000. H_2O diffusion in rhyolitic melts and glasses. Chem. Geol., in press.

Zhang, Y., Belcher, R., Ihinger, P.D., Wang, L., Zhengjiu, X., Newman, S., 1997. New calibration of infrared measurements of dissolved water in rhyolitic glasses. Geochim. Cosmochim. Acta 61, 3089–3100.